International Journal of Radiation Oncology biology • physics

www.redjournal.org

Physics Contribution

Dosimetric Impact of Using the Acuros XB Algorithm for Intensity Modulated Radiation Therapy and RapidArc Planning in Nasopharyngeal Carcinomas

Monica W.K. Kan, MPhil,*,† Lucullus H.T. Leung, PhD,* and Peter K.N. Yu, PhD†

**Department of Oncology, Princess Margaret Hospital, Hong Kong SAR, China; and †Department of Physics and Materials Science, City University of Hong Kong, Hong Kong SAR, China*

Received May 14, 2012, and in revised form Jul 17, 2012. Accepted for publication Aug 21, 2012

Summary

The Acuros XB (AXB) algorithm was proved to calculate more accurate doses than the anisotropic analytical algorithm (AAA) in heterogeneous medium. This investigation was to assess the dosimetric impact of using AXB instead of AAA for the treatment of nasopharyngeal carcinomas, because of the presence of bone and air. Our results proved that AXB estimated lower doses to target volumes and critical organs. The dose reduction was more noticeable in bone than in tissue and air.

Purpose: To assess the dosimetric implications for the intensity modulated radiation therapy (IMRT) and volumetric modulated arc therapy with RapidArc (RA) of nasopharyngeal carcinomas (NPC) due to the use of the Acuros XB (AXB) algorithm versus the anisotropic analytical algorithm (AAA).

Methods and Materials: Nine-field sliding window IMRT and triple-arc RA plans produced for 12 patients with NPC using AAA were recalculated using AXB. The dose distributions to multiple planning target volumes (PTVs) with different prescribed doses and critical organs were compared. The PTVs were separated into components in bone, air, and tissue. The change of doses by AXB due to air and bone, and the variation of the amount of dose changes with number of fields was also studied using simple geometric phantoms.

Results: Using AXB instead of AAA, the averaged mean dose to PTV_{70} (70 Gy was prescribed to PTV_{70}) was found to be 0.9% and 1.2% lower for IMRT and RA, respectively. It was approximately 1% lower in tissue, 2% lower in bone, and 1% higher in air. The averaged minimum dose to PTV_{70} in bone was approximately 4% lower for both IMRT and RA, whereas it was approximately 1.5% lower for PTV_{70} in tissue. The decrease in target doses estimated by AXB was mostly contributed from the presence of bone, less from tissue, and none from air. A similar trend was observed for PTV_{60} (60 Gy was prescribed to PTV_{60}). The doses to most serial organs were found to be 1% to 3% lower and to other organs 4% to 10% lower for both techniques.

Conclusions: The use of the AXB algorithm is highly recommended for IMRT and RapidArc planning for NPC cases.

Introduction

Radiation therapy is one of the main treatment methods for nasopharyngeal carcinomas (NPC). The treatment usually requires sophisticated radiation therapy techniques such as intensity modulated radiation therapy (IMRT) and volumetric modulated arc radiation therapy (1-3).

One of the major limitations of most commercially available correction-based algorithms for photon dose calculation is the

Reprint requests to: Monica W. K. Kan, MPhil, Princess Margaret Hospital, Department of Oncology, Hong Kong SAR, China. Tel: (+852) 2990-2776; Fax: (+852) 2990-2775; E-mail: kanwkm@ha.org.hk

Conflict of interest: none.

Int J Radiation Oncol Biol Phys, Vol. 85, No. 1, pp. e73–e80, 2013
0360-3016/$ - see front matter
http://dx.doi.org/10.1016/j.ijrobp.2012.08.031

ability to account for the effect of electron transport. The commonly used convolution-superposition algorithm, the anisotropic analytical algorithm (AAA), and the collapsed cone convolution algorithm were proved to overestimate the doses near air/tissue interface when small fields were used (4-6). Because the NP region is surrounded by a considerable amount of bony structures and air cavities, the limitations of the algorithms mentioned above may induce errors, therefore affecting the reliability of the calculated patient dose.

Recently a new dose calculation algorithm, the Acuros XB Advanced Dose Calculation (AXB), has been implemented in the Eclipse treatment planning system (Varian Medical Systems, Palo Alto, CA). It explicitly solves the linear Boltzmann transport equation that describes the macroscopic behavior of radiation particles as they travel through and interact with matter. It uses the chemical composition of each material in which particles are transported. Tissue segmentation is based on density ranges related to the Hounsfield units from the CT images, and for each tissue the specific chemical composition is considered according to International Commission on Radiological Protection Report 23 (7). Some recent publications have reported comparable accuracy between AXB and Monte Carlo methods in heterogeneous media (8-11). The main aim of this study was to assess the dosimetric impact on IMRT and RapidArc (RA) for NPC patients due to the recalculation of dose distribution using AXB instead of AAA. In our study the target volumes were stratified into 3 groups: the target in tissue, in bone, and in air. The dosimetric analysis was performed for the original contoured target volumes as well as the stratified target volumes.

The differences in estimating dose distribution with AXB versus AAA were also assessed using simple rectangular phantoms with pure air and pure bone. The dose differences for a single small field and the variation of its effect with increasing field number was also reported. This helps to explain the reasons behind the dose changes due to the presence of bone and air in real patients.

Methods and Materials

Contouring and prescription of target volumes

Twelve NPC patients with staging ranging from T1 to T4 were chosen for this study. The primary gross tumor volume (GTV) covered the gross tumor plus the entire nasopharynx down to the caudal border of the C1 vertebra. The nodal GTV (GTV_N) encompassed any positive lymph nodes defined by a short axis of greater than 1 cm. The boost clinical target volume (CTV_{70}) and the nodal CTV (CTV_N) were formed by adding a 0.5-cm margin to GTV and GTV_N, respectively. The high-risk CTV (CTV_{60}) was created by adding 1 cm margin to CTV_{70} and CTV_N plus minimal coverage for high-risk elective sites. The low-risk CTV (CTV_{54}) covered bilateral level IV and Vb nodal regions unless positive lymph nodes were present where CTV_{60} would extend into level IV and Vb to 0.15 cm below the caudal border of CTV_N. The boost planning target volume (PTV) with nodal PTV (PTV_{70}), high-risk PTV (PTV_{60}), and low-risk PTV (PTV_{54}) were produced by adding 0.3 cm to CTV_{70} with CTV_N, CTV_{60}, and CTV_{54}, respectively. Seventy grays, 60 Gy, and 54 Gy were prescribed to PTV_{70}, PTV_{60}, and PTV_{54}, respectively. The prescription dose was given in 35 daily fractions for T1 or T2 cases and 33 daily fractions for T3 or T4 cases.

The volumes of the contoured PTV_{70} and PTV_{60} include a considerable amount of air cavities and bony structures. To assess the dosimetric impact to PTVs due to materials of different densities, the bony structures and air cavities included in these 2 target volumes were contoured separately as PTV in bone and PTV in air. The rest of the volumes were contoured as PTV in tissue. Little bone and air were found in PTV_{54}, and therefore it was not stratified.

Treatment planning

Intensity modulated radiation therapy plans were created for 12 patients using a 9-field sliding window technique and triple-arc RapidArc. All fields in the IMRT plans were evenly distributed in coplanar beam directions. The triple-arc RA plans were created using 2 complete arcs plus 1 partial arc. All plans were generated using a 6-MV beam and modulated with a 120 multileaf collimator from a linear accelerator (Clinac 23EX; Varian Medical Systems).

All treatment plans were generated using Eclipse, version 10. The optimization goal was to ensure that at least 95% of the PTVs would receive the prescribed reference dose, and no more than 5% of the PTV_{70} would receive 107% of the prescribed dose, while minimizing the doses to organs at risk (OARs). The final dose calculations were performed using AAA version 10.0.28 with inhomogeneity correction and 2.5-mm grid resolution. The quality of each treatment plan was assessed with regard to its clinical acceptability by an oncologist. Each plan was subsequently recalculated using AXB version 10.0.28 with the identical monitor units and multileaf collimator leaf settings as with AAA. Acuros XB using the "dose-to-medium" option with 2.5-mm grid

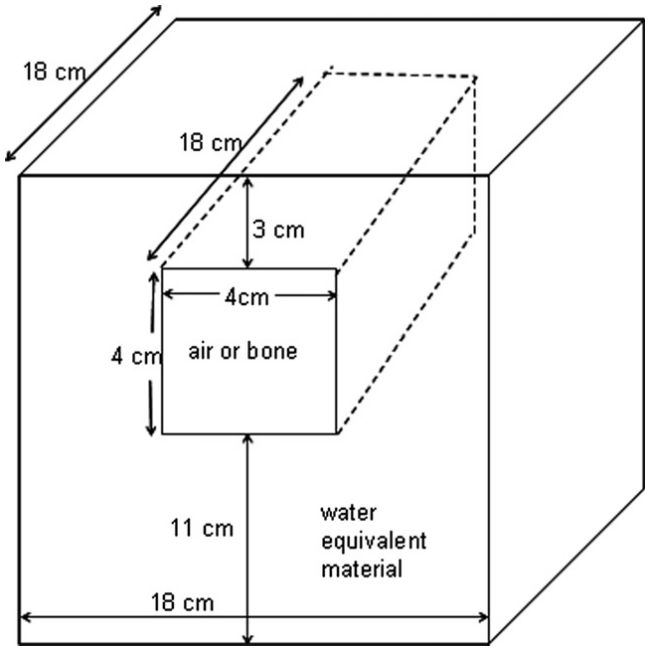

Fig. 1. The tissue equivalent rectangular phantom with air cavity or bone insert for investigation of dose variation due to the use of the Acuros XB algorithm.

Table 1 Summary of averaged doses to target volumes estimated by AAA and AXB over the 12 patients

Item	Parameter	IMRT (AAA)	IMRT (AXB)	P*	RA (AAA)	RA (AXB)	P*
PTV_{70}	$D_{2\%}$, Gy	74.1 ± 0.6	74.0 ± 0.6	~	73.6 ± 0.3	73.6 ± 0.4	~
	$D_{98\%}$, Gy	70.6 ± 0.4	69.3 ± 0.6	+	70.1 ± 0.3	68.8 ± 0.4	+
	Mean, Gy	72.5 ± 0.5	71.8 ± 0.6	+	72.2 ± 0.2	71.4 ± 0.2	+
	$V_{>107}$, %	1.1 ± 3.3	0.9 ± 2.1	~	0.0 ± 0.1	0.1 ± 0.1	+
	$V_{>95}$, %	100 ± 0.0	100 ± 0.0	~	100 ± 0.0	100 ± 0.1	~
	HI	0.049 ± 0.005	0.066 ± 0.007	+	0.048 ± 0.008	0.067 ± 0.008	+
	CN	0.81 ± 0.04	0.81 ± 0.03	~	0.85 ± 0.02	0.82 ± 0.03	+
PTV_{70}_tissue	$D_{2\%}$, Gy	74.1 ± 0.6	73.8 ± 0.7	+	73.7 ± 0.3	73.3 ± 0.3	+
	$D_{98\%}$, Gy	70.7 ± 0.4	69.8 ± 0.5	+	70.4 ± 0.4	69.3 ± 0.4	+
	Mean, Gy	72.5 ± 0.5	71.8 ± 0.6	+	72.3 ± 0.2	71.4 ± 0.2	+
	$V_{>95}$, %	100 ± 0.0	100 ± 0.0	~	100 ± 0.0	100 ± 0.0	~
	HI	0.047 ± 0.005	0.056 ± 0.005	+	0.045 ± 0.008	0.056 ± 0.006	+
PTV_{70}_bone	$D_{2\%}$, Gy	74.1 ± 0.6	73.1 ± 0.6	+	73.6 ± 0.4	72.3 ± 0.4	+
	$D_{98\%}$, Gy	70.6 ± 0.5	67.9 ± 0.7	+	70.3 ± 0.4	67.6 ± 0.5	+
	Mean, Gy	72.5 ± 0.4	71.0 ± 0.6	+	72.2 ± 0.3	70.5 ± 0.4	+
	$V_{>95}$, %	100 ± 0.0	99.8 ± 0.2	+	100 ± 0.0	99.6 ± 0.3	+
	HI	0.049 ± 0.005	0.072 ± 0.008	+	0.046 ± 0.007	0.067 ± 0.008	+
PTV_{70}_air	$D_{2\%}$, Gy	73.4 ± 0.4	74.7 ± 0.6	+	72.9 ± 0.4	74.4 ± 0.5	+
	$D_{98\%}$, Gy	70.5 ± 0.4	71.3 ± 0.6	+	70.1 ± 0.4	70.8 ± 0.4	+
	Mean, Gy	71.9 ± 0.3	73.0 ± 0.5	+	71.8 ± 0.3	72.7 ± 0.4	+
	$V_{>95}$, %	100 ± 0.0	100 ± 0.0	~	100 ± 0.0	100 ± 0.0	~
	HI	0.040 ± 0.005	0.047 ± 0.005	+	0.039 ± 0.008	0.049 ± 0.008	+
PTV_{60}	$D_{2\%}$, Gy	73.6 ± 0.6	73.2 ± 0.7	+	73.2 ± 0.3	72.7 ± 0.4	+
	$D_{98\%}$, Gy	60.9 ± 0.4	60.1 ± 0.5	+	60.1 ± 0.5	59.3 ± 0.4	+
	Mean, Gy	66.9 ± 0.9	66.2 ± 1.0	+	66.9 ± 0.4	66.0 ± 0.5	+
	$V_{>95}$, %	100.0 ± 0.1	99.9 ± 0.1	~	99.8 ± 0.2	99.7 ± 0.2	~
	HI	0.191 ± 0.009	0.198 ± 0.009	~	0.197 ± 0.009	0.204 ± 0.008	~
	CN	0.84 ± 0.03	0.85 ± 0.03	~	0.86 ± 0.02	0.88 ± 0.02	~
PTV_{60}_tissue	$D_{2\%}$, Gy	73.5 ± 0.6	73.0 ± 0.7	+	73.2 ± 0.3	72.5 ± 0.3	+
	$D_{98\%}$, Gy	61.0 ± 0.4	60.3 ± 0.5	+	60.3 ± 0.6	59.7 ± 0.5	+
	Mean, Gy	66.8 ± 0.9	66.1 ± 1.0	+	66.9 ± 0.4	65.9 ± 0.4	+
	$V_{>95}$, %	100 ± 0.1	99.9 ± 0.1	+	99.8 ± 0.2	99.8 ± 0.2	~
	HI	0.190 ± 0.008	0.193 ± 0.009	~	0.194 ± 0.011	0.195 ± 0.008	~
PTV_{60}_bone	$D_{2\%}$, Gy	73.7 ± 0.5	72.6 ± 0.6	+	73.3 ± 0.5	71.9 ± 0.5	+
	$D_{98\%}$, Gy	61.2 ± 0.4	59.1 ± 0.6	+	60.5 ± 0.5	58.4 ± 0.6	+
	Mean, Gy	68.2 ± 0.9	66.6 ± 0.9	+	68.2 ± 1.4	66.1 ± 0.7	+
	$V_{>95}$, %	100 ± 0.0	99.7 ± 0.2	+	99.9 ± 0.1	99.3 ± 0.4	+
	HI	0.185 ± 0.009	0.202 ± 0.012	+	0.187 ± 0.009	0.204 ± 0.011	+
PTV_{60}_air	$D_{2\%}$, Gy	73.0 ± 0.4	74.2 ± 0.5	+	72.7 ± 0.5	73.8 ± 0.5	+
	$D_{98\%}$, Gy	60.7 ± 0.5	60.9 ± 0.8	~	60.3 ± 0.6	60.1 ± 1.1	~
	Mean, Gy	66.7 ± 1.4	67.7 ± 1.4	+	66.7 ± 1.1	67.5 ± 1.1	+
	$V_{>95}$, %	100 ± 0.1	100.0 ± 0.1	~	100 ± 0.1	99.8 ± 0.3	~
	HI	0.187 ± 0.011	0.199 ± 0.014	+	0.188 ± 0.012	0.204 ± 0.020	+
PTV_{54}	$D_{2\%}$, Gy	61.1 ± 2.5	61.1 ± 2.6	~	60.8 ± 2.2	60.3 ± 2.3	~
	$D_{98\%}$, Gy	54.7 ± 0.6	54.2 ± 0.7	+	53.9 ± 0.6	53.6 ± 0.5	+
	Mean, Gy	57.3 ± 0.6	57.0 ± 0.7	+	57.2 ± 0.4	56.6 ± 0.4	+
	$V_{>95}$, %	100 ± 0.05	100 ± 0.05	~	99.9 ± 0.1	99.9 ± 0.1	~
	HI	0.113 ± 0.045	0.120 ± 0.048	~	0.121 ± 0.040	0.119 ± 0.044	~

Abbreviations: AAA = anisotropic analytical algorithm; AXB = Acuros XB algorithm; CN = confirmation number; HI = homogeneity index; IMRT = intensity modulated radiation therapy; RA = RapidArc.

* The symbol "+" stands for a P value ≤.05 for which the result is statistically significant, and the symbol "~" stands for a P value >.05.

resolution was used. Two options of dose reporting modes were available in AXB: dose-to-water (D_w) and dose-to-medium (D_m). Both calculate the energy-dependent electron fluence according to the material properties of the media. The difference between these 2 options is in the postprocessing step, during which the energy-dependent fluence calculated by AXB's transport is multiplied by different flux-to-dose response functions to obtain the absorbed dose. For D_m, AXB uses a medium-based response function, whereas for D_w AXB uses a water-based response function (8-11).

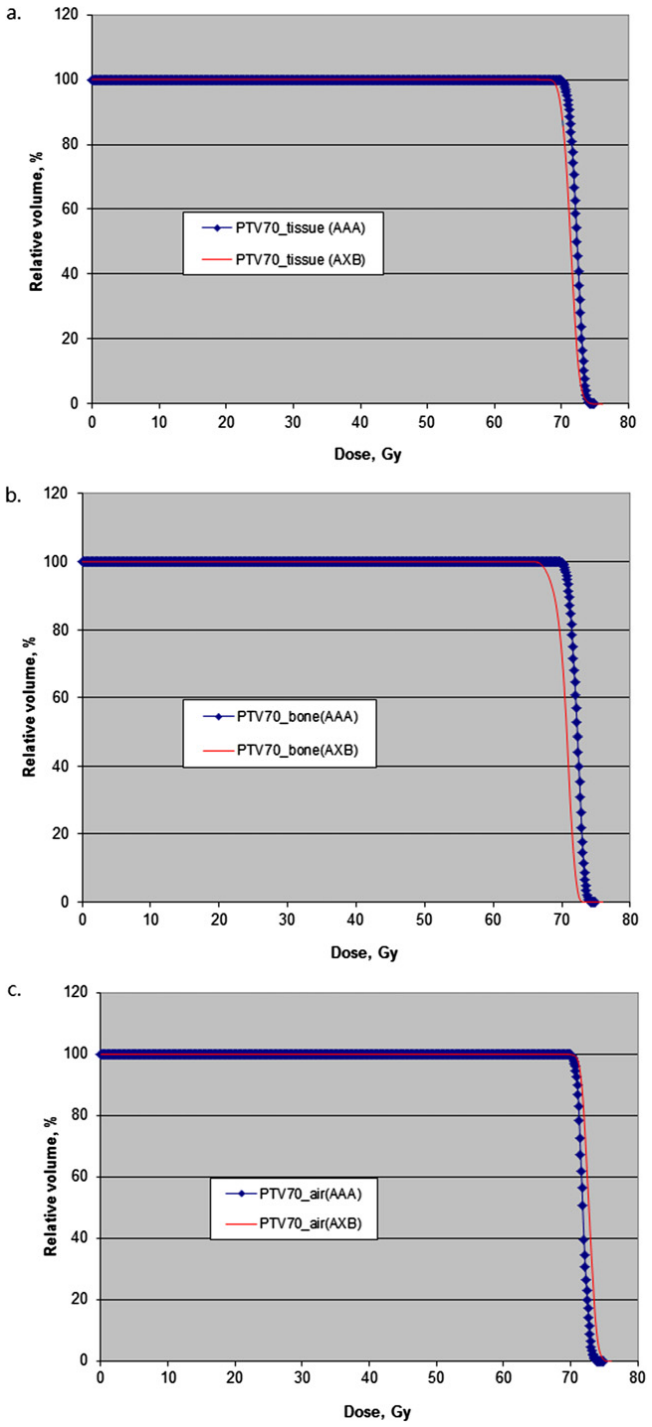

Fig. 2. Comparison of the dose-volume histograms estimated using the Acuros XB algorithm (AXB) and the anisotropic analytical algorithm (AAA) for different components of the planning target volume (PTV) in (a) tissue, (b) bone, and (c) air for a typical intensity modulated radiation therapy plan.

Dosimetric evaluation

For the originally contoured PTVs and those corresponding separated components in bone (PTV_bone), air (PTV_air), and tissue (PTV_tissue), doses were calculated using AAA and AXB and compared in terms of the mean doses, maximum doses represented by $D_{2\%}$ (minimum doses received by 2% of the target volumes), and minimum doses represented by $D_{98\%}$. The coverage to targets represented by $V_{>95\%}$ (volume receiving more than 95% of the reference dose) and the hot areas represented by $V_{>107\%}$ were compared. Target dose homogeneity was evaluated by using the homogeneity index (HI), defined as the ratio $(D_{2\%}\text{-}D_{98\%})/D_{50\%}$ (12). A lower HI indicates a more homogeneous target dose. The plan conformity was also evaluated using the confirmation number, which was defined as the product of $V_{T,\,ref}/V_T$ and $V_{T,\,ref}/V_{ref}$, where $V_{T,\,ref}$ represents the volume of the target receiving a dose equal to or greater than the prescribed dose, V_T represents the physical volume of the target, and V_{ref} represents the total tissue volume receiving a dose equal to or greater than the prescribed dose (13).

Clinically relevant OAR dose parameters were compared. The parameters studied include the dose encompassing 1% ($D_{1\%}$) and 5% ($D_{5\%}$) of the volume for brain stem, spinal cord, optic chiasm, optic nerve, temporal lobes, and brachial plexus. The differences in mean doses to all the above-mentioned serial organs as well as mean doses to lens, eyes, inner ears, parotid glands, mandible, and pituitary were reported. Besides, the volumes of parotid glands receiving more than 30 Gy ($V_{30\ Gy}$) were also reported. The Wilcoxon matched-pair signed rank test was used to compare the results. The threshold for statistical significance was $P<.05$. All statistical tests were 2-sided and were performed using the Statistical Package for Social Sciences, version 11.0 (SPSS, Chicago, IL).

Dose effect in simple geometric phantom

To have a better understanding of the dose changes due to the presence of air and its variation with increasing field numbers, a tissue equivalent rectangular phantom with air cavity only was constructed to investigate the differences between AXB and AAA. The shape and dimensions of the phantom are shown in Figure 1. The central axis depth doses and dose profiles in the middle of air and at the air/tissue interfaces from a single small field of $3 \times 15\ cm^2$ were calculated and compared between AXB and AAA using the same monitor unit settings. The air cavity and the surrounding tissue equivalent material with 5-mm margin were subsequently contoured as 2 different organs. The ratio of mean dose to each organ calculated by AXB to that by AAA was estimated for plans with increasing number of fields, ranging from 1 to 10, using the same field size ($3 \times 15 cm^2$) coming from evenly distributed directions. The same ratio was also calculated for one IMRT plan and one RA plan for NPC. The isocenter of each plan was located 7 cm below the phantom surface at the middle of the air/tissue interface. The dose variation due to bone was also studied by repeating the same procedures and replacing the air cavity with bone.

Results

Doses to real patients

Table 1 summarizes the doses, homogeneity, and conformity to PTVs of different components in air, bone, and tissue averaged over the 12 patients. For IMRT plans, it can be observed that the mean dose to PTV_{70} estimated by AXB compared with AAA were 0.9% lower. It was 1% lower for PTV_{70}_tissue, 2% lower for

Table 2 Summary of averaged doses to organs at risk estimated by AAA and AXB over the 12 patients

Item	Parameter	IMRT (AAA)	IMRT (AXB)	P*	RA (AAA)	RA (AXB)	P*
Brain stem	$D_{1\%}$, Gy	49.8 ± 1.6	49.2 ± 1.6	+	49.8 ± 1.4	49.0 ± 1.3	+
	$D_{5\%}$, Gy	47.4 ± 1.7	46.8 ± 1.8	+	47.8 ± 1.6	47.0 ± 1.5	+
	Mean, Gy	30.9 ± 3.8	30.4 ± 3.8	+	33.2 ± 4.1	32.2 ± 4.1	+
Spinal cord	$D_{1\%}$, Gy	41.7 ± 1.8	41.0 ± 1.9	+	40.5 ± 0.9	39.6 ± 0.8	+
	$D_{5\%}$, Gy	40.6 ± 1.7	40.0 ± 1.8	+	39.4 ± 0.9	38.6 ± 0.9	+
	Mean, Gy	32.4 ± 3.3	31.8 ± 3.3	+	33.2 ± 2.8	32.5 ± 2.7	~
Optic chiasm	$D_{1\%}$, Gy	23.4 ± 19.5	23.0 ± 19.8	+	24.7 ± 18.8	24.1 ± 18.8	+
	$D_{5\%}$, Gy	22.5 ± 19.6	22.1 ± 19.8	+	23.7 ± 18.7	23.0 ± 18.7	+
	Mean, Gy	17.3 ± 16.7	16.9 ± 16.8	+	18.8 ± 16.3	18.2 ± 16.3	+
Optic nerve	$D_{1\%}$, Gy	24.7 ± 20.6	24.3 ± 20.8	+	24.7 ± 18.8	24.1 ± 18.9	+
	$D_{5\%}$, Gy	22.8 ± 20.2	22.3 ± 20.4	+	22.3 ± 18.6	19.6 ± 18.5	+
	Mean, Gy	14.0 ± 11.7	13.5 ± 11.8	+	13.8 ± 10.7	11.4 ± 10.6	+
Temporal lobe	$D_{1\%}$, Gy	63.1 ± 3.7	62.8 ± 3.7	+	63.3 ± 3.4	63.0 ± 3.4	+
	$D_{5\%}$, Gy	51.7 ± 6.4	51.4 ± 6.3	+	47.7 ± 6.8	47.4 ± 6.8	+
	Mean, Gy	17.2 ± 4.5	16.9 ± 4.4	+	16.8 ± 4.5	16.5 ± 4.5	+
Brachial plexus	$D_{1\%}$, Gy	61.5 ± 1.1	60.8 ± 1.2	+	61.1 ± 0.9	60.1 ± 0.8	+
	$D_{5\%}$, Gy	59.5 ± 2.1	58.8 ± 2.1	+	59.4 ± 1.7	58.4 ± 1.7	+
	Mean, Gy	36.5 ± 7.7	36.1 ± 7.6	+	37.1 ± 7.8	36.6 ± 7.6	+
Parotid gland	Mean, Gy	30.2 ± 3.9	29.4 ± 3.9	+	28.2 ± 2.8	27.2 ± 2.8	+
	$V_{>30}$, %	38.3 ± 10.1	36.8 ± 9.4	+	34.1 ± 6.7	32.0 ± 6.5	+
Lens	Mean, Gy	3.9 ± 0.5	3.4 ± 0.4	+	4.9 ± 0.9	4.2 ± 0.9	+
Eye	Mean, Gy	6.3 ± 1.8	5.9 ± 1.7	+	7.0 ± 2.1	6.6 ± 2.0	+
Inner ear	Mean, Gy	48.7 ± 5.4	46.7 ± 5.2	+	46.6 ± 5.1	44.4 ± 4.9	+
Pituitary	Mean, Gy	44.4 ± 14.0	44.5 ± 14.2	~	43.7 ± 12.6	43.3 ± 12.7	+
Mandible	Mean, Gy	45.5 ± 3.2	44.0 ± 3.2	+	46.7 ± 3.0	45.1 ± 2.9	+

Abbreviations as in Table 1.

* The symbol "+" stands for a P value $\leq$.05 for which the result is statistically significant, and the symbol "~" stands for a P value $>$.05.

PTV_{70}_bone, and 1.5% higher for PTV_{70}_air. The averaged minimum dose to PTV_{70} was 1.8% lower. It was 1.4% lower for PTV_{70}_tissue, 3.7% lower for PTV_{70}_bone, and 1.1% higher for PTV_{70}_air. The reduction of doses predicted by AXB to PTV_{70}_bone was relatively more than those in PTV_{70}_tissue, whereas slightly higher doses were observed in PTV_{70}_air. The higher HI values calculated by AXB for PTV_{70} indicated a less homogeneous dose. For bone and tissue, AXB predicted more dose reduction in $D_{98\%}$ than in $D_{2\%}$, indicating an increase in cold areas and negligible change in hot areas in the target. For air, AXB predicted both higher $D_{2\%}$ and $D_{98\%}$ values, with more increase in $D_{2\%}$, indicating more hot areas. There was negligible difference in the conformity and coverage represented by $V_{>95\%}$ between AXB and AAA. Similar changes in the mean and minimum doses were observed for PTV_{60}. A very similar trend was observed for the target volumes for RA plans. Figure 2 shows the dose-volume histogram for the different PTV components of a typical IMRT plan.

Table 2 summarizes the doses to OARs averaged over the 12 patients. For IMRT plans, the doses represented by $D_{1\%}$ to serial organs including brain stem, spinal cord, optic nerves, optic chiasm, and brachial plexus were 1% to 2% lower (ie, approximately 0.4-0.7 Gy) estimated by AXB compared with AAA. Using AXB, the estimated mean doses to lens and eyes were 11% and 6% lower, with the actual reduction in doses less than 0.5 Gy. The mean doses to parotid were decreased by approximately 0.8 Gy, with an approximately 1.5% decrease in the volume of $V_{30\ Gy}$. There was little dose reduction in temporal lobe and pituitary. Slightly more reduction in the mean doses was observed in OARs with a high proportion of bony structures, such as mandible and inner ears. It was 2 Gy for inner ears and 1.5 Gy for mandible. A very similar trend was observed for the OARs for RA plans.

Dose variation due to air and bone in simple geometric phantom

The central axis depth doses and dose profiles in air and bone, as well as near air/tissue and bone/tissue interfaces, calculated by AXB and AAA are shown in Figure 3. It was observed from the depth dose curves that AXB predicted lower doses in air and more severe secondary build-up beyond air. The dose profiles in air and near the air/tissue interfaces also indicated lower doses inside the field but higher out-of-field doses predicted by AXB. The depth dose curves in the bone phantom indicated lower doses within bone predicted by AXB. The dose profiles in bone and at the bone/tissue interface indicated lower doses inside the field.

The variation of the ratio of mean doses to air, bone, and the nearby tissues calculated by AXB versus AAA with the number of fields is shown in Figure 4. For the plans with air it can be seen that this ratio of mean dose in air, $R_{air(AxB/AAA)}$, increased as the number of field increased and became greater than 1 for IMRT and RA plans, indicating that slightly higher doses would appear in air predicted by AXB. The ratio for the nearby tissue increased dramatically, from 0.78 to 0.98, by switching from 1 field to 2 fields, and approaches to 0.99 when 7 fields are used. For the plans with bone, the ratio, $R_{bone(AxB/AAA)}$, slightly increased from 0.91 to 0.95 when switching from 1 field to 2 fields and then

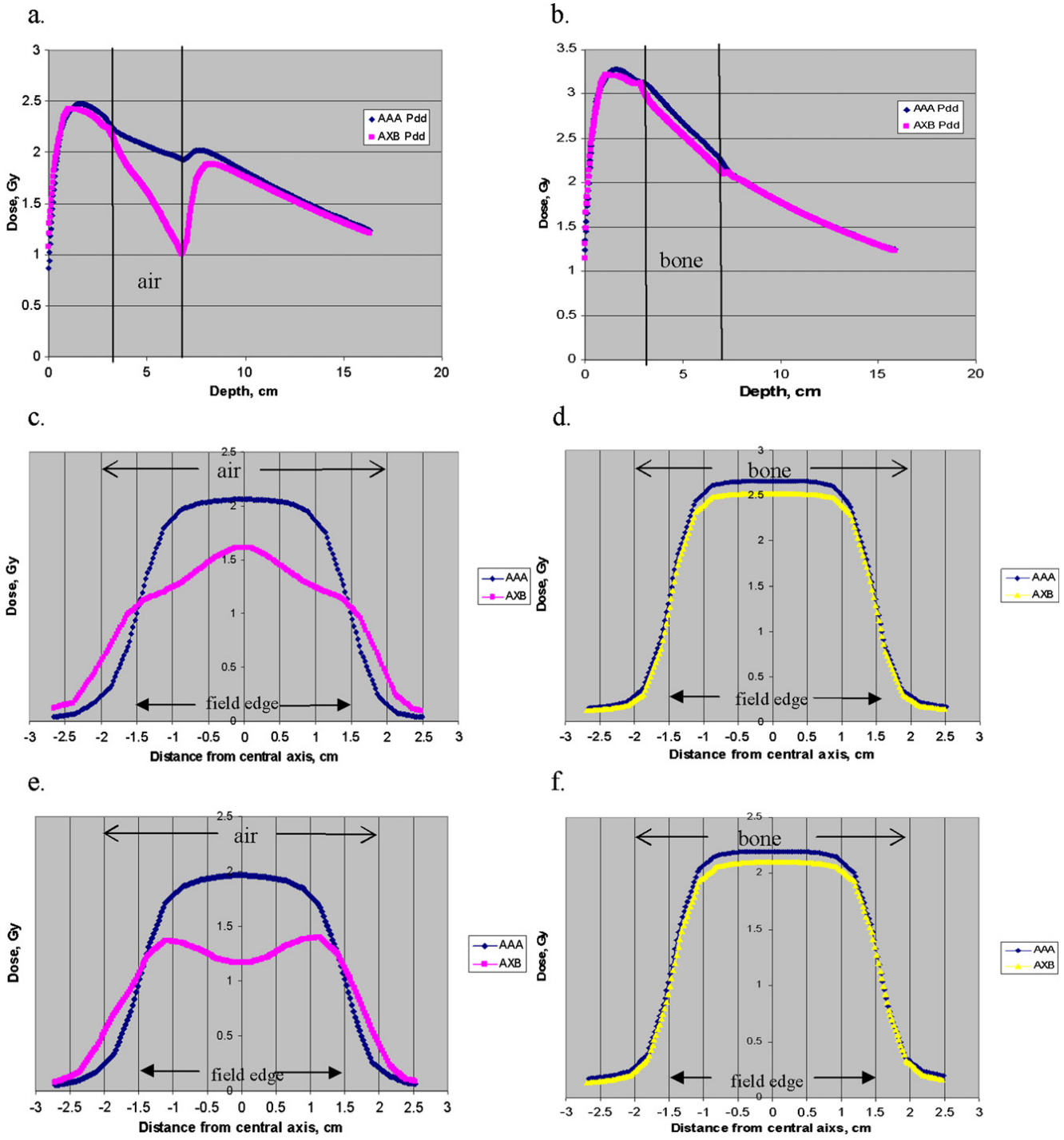

Fig. 3. Central axis depth doses estimated in the rectangular phantom with the presence of (a) air and (b) bone, together with dose profiles estimated in the middle of (c) air and (d) bone, and also at the (e) air/tissue and (f) bone/tissue distal interfaces beyond air/bone insert by the anisotropic analytical algorithm (AAA) and the Acuros XB algorithm (AXB) for a single small 3 × 15-cm^2 field.

became almost constant with more fields; it remained to be approximately 0.95 even for IMRT and RA. The ratio of the nearby tissue around bone demonstrated a similar trend as those around air.

Discussion

Previous investigations assessing the clinical impact of AXB in non-small cell lung cancer reported lower mean dose in soft tissue and slightly higher mean dose in low-density lung tissue for 6-MV beams predicted by AXB compared with AAA. As in the present investigations, they found no systematic differences related to the treatment techniques (14). Another analysis in breast treatment reported a reduction of approximately 1 Gy to the muscle tissue by using AXB instead of AAA (15). Our results showed that there was a reduction in the mean PTV doses in tissue and in bone. It was believed these changes were the result of the AXB's improved modeling of the radiation transport in medium. Previous investigations in heterogeneous phantoms compared with the

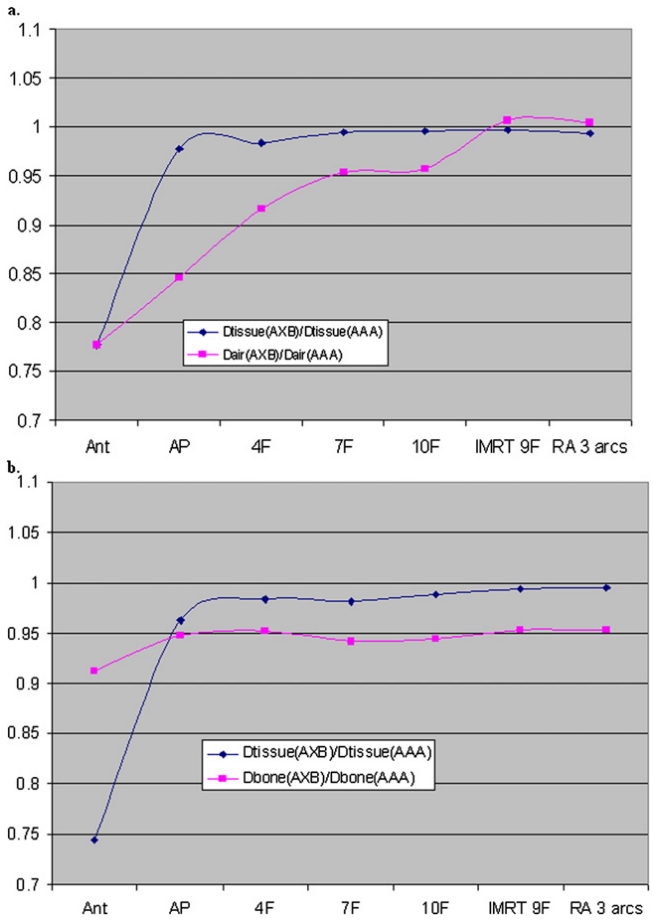

Fig. 4. Variation of the ratios of mean doses to air, bone, and the nearby tissues calculated by the Acuros XB algorithm (AXB) versus the anisotropic analytical algorithm (AAA) with the number of fields (F). Ant = single anterior field; AP = anterior posterior opposing fields; IMRT = intensity modulated radiation therapy; RA = RapidArc.

Monte Carlo methods proved that AXB was more accurate than AAA (8-11).

The dosimetric effect due to air cavity is one of the major concerns for NPC cases. The AAA assumed independently scaled depth-directed and lateral components for heterogeneity correction. The depth-directed component is scaled by taking into account the radiologic distance between the surface and the point of interest, whereas the scatter kernel is scaled by calculating the water equivalent path length radially from the center of the beamlet. The divergent scatter of heterogeneities from upper levels was not taken into account correctly. The AXB was able to describe the interactions of radiation particles with matter on the basis of approximate numerical methods and performed dose calculations using the material composition of each voxel derived from the CT data. Our simple phantom study has shown that AXB predicts much more secondary build-up and therefore much lower doses beyond the air/tissue interfaces than AAA along the central axis from a single small 6-MV beam (9, 10). On the other hand, the dose profiles predicted by AXB indicated higher out-of-field doses in air and near air/tissue interface due to the increased lateral electron transport from the field center. Our phantom study showed that the effect of dose reduction in air and near air/tissue interfaces due to secondary build-up near the field center significantly decreased as the number of fields increased. This is reflected from the ratios $R_{air(AAA/AxB)}$ and $R_{tissue(AAA/AxB)}$. The ratio $R_{tissue(AAA/AxB)}$ increased to 0.99 as the number of fields increased, and $R_{air(AAA/AxB)}$ was even greater than 1 for IMRT and RA plans. This is because part of the reduction from each single field was compensated by the increase in out-of-field doses from other fields coming from different directions. For IMRT, the reduction of doses due to re-build-up from one small field segment would be partly compensated by adjacent segments of the same field direction. For RA plans, each arc can be considered as composed of a very large number of static fields.

The dose effect due to bone is another concern in this study. Our investigation using a rectangular phantom with bone for a single field showed lower doses predicted by AXB in bone content. Unlike the dose effect due to air, the dose reduction in bone only occurred inside the field and was not compensated by the effect of multiple field directions. Similar to most of the other model-based algorithms, AAA computed and reported the absorbed dose as if it were deposited in water. It used electron density to scale the dose kernel for photon scatter along the beamlet direction in heterogeneous media. The AXB calculated dose considering the elemental composition. Unlike most water-like tissues in the body, such as muscle and lung, the elemental composition of compact bone is quite different from that of water. Previous studies proved that dose calculations neglecting the elemental composition induced negligible effect in lighter tissue but not in compact bone (16). Our results found approximately 4% reduction of minimum doses recalculated by AXB in the bony content of the PTVs. The bony content contoured in the PTVs included both soft and compact bones. The amount of dose reduction in soft bone would be smaller than that of the compact bone; therefore, the reduction of maximum doses was only approximately 1%, resulting in less dose homogeneity predicted by AXB. Dose calculations with the rectangular phantom showed slightly lower doses to the nearby tissues predicted by AXB. This might be due to the smaller exit doses from bone and partly explains the 1% lower mean doses to PTV in tissue.

If oncologists kept using the original dose prescription and accepting criteria of plan quality when switching from AAA to AXB, a maximum of up to approximately 4% more radiation doses would be given to the bony content of the PTVs, because calculations from AXB would require more radiation output to produce the same coverage as AAA. Some of the bony structures were included in the region of heavy tumor burden. There is a possibility that the local control of the tumor might be improved. However, this requires further clinical investigations with long-term follow-up for NPC patients.

Conclusion

The AXB algorithm should be used in preference to AAA for cases in which PTVs are involved with tissues of highly different densities, such as NPC.

References

1. Doornaert P, Verbakel W, Bieker M, et al. RapidArc planning and dlivery in patients with locally advanced head and neck cancer undergoing chemoradiotherapy. *Int J Radiat Oncol Biol Phys* 2011;79: 429-435.
2. Lai SZ, Li WF, Chen L, et al. How does intensity-modulated radiotherapy versus conventional two-dimensional radiotherapy influence

the treatment results in nasopharyngeal carcinoma patients? *Int J Radiat Oncol Biol Phys* 2011;80:661-668.
3. Su SF, Han F, Zhao C, et al. Long-term outcomes of early-stage nasopharyngeal carcinoma patients treated with intensity-modulated radiotherapy alone. *Int J Radiat Oncol Biol Phys* 2012; 82:327-333.
4. Arnfield M, Siantar C, Siebers J, et al. The impact of electron transport on the accuracy of computed dose. *Med Phys* 2000;27:1266-1273.
5. Tillikainen L, Helminen H, Torsti T, et al. A 3D pencil-beam-based superposition algorithm for photon dose calculation in heterogeneous media. *Phys Med Biol* 2008;53:3821-3839.
6. Kan WK, Cheung YC, Leung HT, et al. The accuracy of dose calculations by anisotropic analytical algorithms for stereotactic radiotherapy in nasopharyngeal carcinoma. *Phys Med Biol* 2011;56: 397-413.
7. International Commission on Radiological Protection. International Commission on Radiological Protection Report 23. Reference Man: Anatomical, Physiological and Metabolic Characteristics. New York: ICRP; 1975.
8. Vassiliev O, Wareing T, McGhee J, et al. Validation of a new grid based Blotzmann equation solver for dose calculation in radiotherapy with photon beams. *Phys Med Biol* 2010;55:581-598.
9. Fogliata A, Nicolini G, Clivio A, et al. Dosimetric evaluation of Acuros XB Advanced Dose Calculation algorithm in heterogeneous media. *Radiat Oncol* 2011;6:82.
10. Bush K, Gagne S, Zavgorodni W, et al. Dosimetric validation of Acuros XB with Monte Carlo methods for photon dose calculations. *Med Phys* 2011;38:2208-2221.
11. Han T, Mikell J, Salehpour M, et al. Dosimetric comparison of Acuros XB deterministic radiation transportmethod with Monte Carlo and model-based convolution methods in heterogeneous media. *Med Phys* 2011;38:2651-2664.
12. International Commission on Radiation Units and Measurement. Prescribing, Recording, and Reporting Photon-Beam Intensity-Modulation Radiation Therapy (IMRT). Oxford: ICRU; 2010. ICRU Report 83.
13. Van't Riet A, Mak AC, Moerland MA, et al. A conformation number to quantify the degree of conformality in brachytherapy and external beam irradiation: Application to the prostate. *Int J Radiat Oncol Biol Phys* 1997;37:731-736.
14. Fogliata A, Nicolini G, Clivio A, et al. Critical appraisal of Acuros XB and anisotropic analytic algorithm dose calculation in advanced non-small-cell lung cancer treatments. *Int J Radiat Oncol Biol Phys* 2012;83:1587-1595.
15. Fogliata A, Nicolini G, Clivio A, et al. On the dosimetric impact of inhomogeneity management in the Acuros XB algorithm for breast treatment. *Radiat Oncol* 2011;6:103.
16. Siebers V, Keall PJ, Nahum AE, et al. Converting absorbed dose to medium to absorbed dose to water for Monte Carlo based photon beam dose calculations. *Phys Med Biol* 2000;45:983-995.